Effect of Exchange Interaction on Spin Dephasing in a Double Quantum Dot

E. A. Laird,[1] J. R. Petta,[1] A. C. Johnson,[1] C. M. Marcus,[1] A. Yacoby,[2] M. P. Hanson,[3] and A. C. Gossard[3]

[1]*Department of Physics, Harvard University, Cambridge, Massachusetts 02138, USA*

[2]*Department of Condensed Matter Physics, Weizmann Institute of Science, Rehovot 76100, Israel*

[3]*Materials Department, University of California at Santa Barbara, Santa Barbara, California 93106, USA*

(Received 3 December 2005; published 31 July 2006)

We measure singlet-triplet dephasing in a two-electron double quantum dot in the presence of an exchange interaction which can be electrically tuned from much smaller to much larger than the hyperfine energy. Saturation of dephasing and damped oscillations of the spin correlator as a function of time are observed when the two interaction strengths are comparable. Both features of the data are compared with predictions from a quasistatic model of the hyperfine field.

DOI: 10.1103/PhysRevLett.97.056801 PACS numbers: 73.21.La, 71.70.Gm, 71.70.Jp

Implementing quantum information processing in solid-state circuitry is an enticing experimental goal, offering the possibility of tunable device parameters and straightforward scaling. However, realization will require control over the strong environmental decoherence typical of solid-state systems. An attractive candidate system uses electron spin as the holder of quantum information [1,2]. In III-V semiconductor quantum dots, where the highest degree of spin control has been achieved [3–9], the dominant decoherence mechanism is hyperfine interaction with the lattice nuclei [10]. A recent experiment [9] studied this decoherence in a qubit encoded in a pair of spins [11]. In this situation, the dynamics are governed by two competing effects: the hyperfine interaction, which tends to mix the singlet and triplet basis states, and exchange, which tends to preserve them.

The interplay of hyperfine and exchange effects has been studied recently via spin-blockaded transport in two double-dot systems [12,13]. Oscillations and bistability [12] of the leakage current, as well as suppression of mixing with stronger exchange [13] were observed. The topic also has a long history in physical chemistry: recombination of a radical pair created in a triplet state proceeds significantly faster for radicals containing isotopes whose nuclei carry spin [14]. By lifting the singlet-triplet degeneracy, the exchange interaction suppresses spin transitions; its strength can be deduced from the magnetic field dependence of the recombination rate [15]. However, exchange is difficult to tune *in situ* in chemical systems.

In this Letter, singlet correlations between two separated electrons in a GaAs double-dot system are measured as a function of a gate-voltage tunable exchange J and as a function of time τ_S following the preparation of an initial singlet. This study gives insight into the interplay of local hyperfine interactions and exchange in a highly controllable quantum system. We measure the probability $P_S(\tau_S)$ that an initial singlet will be detected as a singlet after time τ_S for J ranging from much smaller than to much greater than the rms hyperfine interaction strength in each dot, E_{nuc}. When $J \ll E_{\mathrm{nuc}}$, we find that P_S decays on a time scale $T_2^* \equiv \hbar/E_{\mathrm{nuc}} = 14$ ns. In the opposite limit where exchange dominates, $J \gg E_{\mathrm{nuc}}$, we find that singlet correlations are substantially preserved over hundreds of nanoseconds. In the intermediate regime, where $J \sim E_{\mathrm{nuc}}$, we observe oscillations in P_S that depend on the ratio E_{nuc}/J. Our results show that a finite exchange energy can be used to extend spin correlations for times well beyond T_2^*.

These observations are in reasonable agreement with recent theory, which predicts a singlet probability (assuming perfect readout) $P_S^0(\tau_S)$ that exhibits damped oscillations as a function of time and a long-time saturation that depends solely on the ratio E_{nuc}/J [16]. To compare experiment and theory quantitatively we introduce an empirical visibility, V, to account for readout inefficiency, $P_S(\tau_S) = 1 - V[1 - P_S^0(\tau_S)]$.

The device used in the experiment, shown in Fig. 1(a), is fabricated on a $GaAs/Al_{0.3}Ga_{0.7}As$ heterostructure with a two-dimensional electron gas (density 2×10^{15} m^{-2}, mobility 20 m^2/V s) 100 nm below the surface. Ti/Au top gates define a few-electron double quantum dot. The interdot tunnel coupling t_c and $(0, 2)$-$(1, 1)$ detuning ϵ are also separately tunable. A charge-sensing quantum point contact with conductance $g_s \sim 0.2e^2/h$ allows the occupancy of each dot to be separately measured [17,18]. We monitor g_s using a lock-in amplifier with a 1 nA current bias at 335 Hz, with a 30 ms time constant.

Measurements were made in a dilution refrigerator at electron temperature $T_e \approx 100$ mK measured from the width of the $(1, 1)$-$(0, 2)$ transition [19]. Gates L and R (see Fig. 1) were connected via filtered coaxial lines to the outputs of a Tektronix AWG520. We report measurements for two settings of tunneling strength, controlled using voltages on gate T and measured from the width of the $(1, 1)$-$(0, 2)$ transition: $t_c \approx 23$ μeV ("large t_c") and $t_c < 9$ μeV ("small t_c") [19]. Except where stated, measurements were made in a perpendicular magnetic field of 200 mT, corresponding to a Zeeman energy $E_Z = 5$ μeV $\gg E_{\mathrm{nuc}}$.

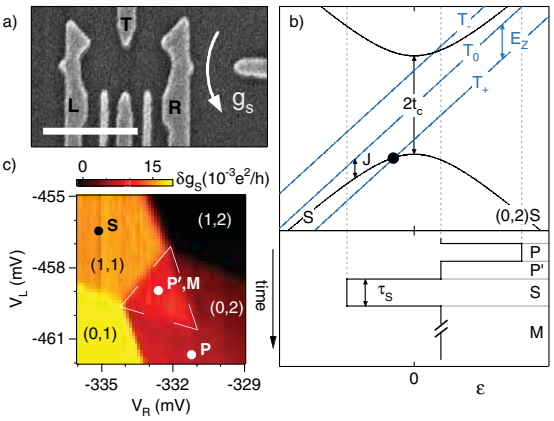

FIG. 1 (color). (a) Micrograph of a device with the same gate design as the one measured (scale bar = 500 nm). Voltages applied to gates L and R adjust the double-dot detuning, ϵ. Gate T sets the interdot tunnel coupling. The conductance g_s of a nearby sensor quantum point contact monitors the average occupation of each dot. (b) Upper panel: Level diagram for the double dot near the (1, 1)-(0, 2) transition ($\epsilon = 0$) plotted versus ϵ. Exchange (J) and Zeeman (E_Z) energies are indicated. The symbol ● denotes the S-T_+ degeneracy. Labels (m, n) denote the occupancies of the left and right dot, respectively. Lower panel: The pulse scheme, consisting of prepare (P, P'), separate (S), and measure (M) steps. Approximately 90% of the cycle is spent in M. (c) g_s close to the (1, 1)-(0, 2) transition during application of pulses, showing the pulse triangle (marked) and the positions of points P, P', S, and M. A background plane has been subtracted.

Figure 1(b) shows the relevant energy levels near the (1, 1)-(0, 2) charge transition as a function of energy detuning ϵ between these charge states. With $t_c = 0$, the (1, 1) singlet S and $m_s = 0$ triplet T_0 are degenerate; the $m_s = \pm 1$ triplets $T_\pm$ are split off in energy from T_0 by $\mp E_Z$. Finite t_c leads to hybridization of the (0, 2) and (1, 1) singlets, inducing an exchange splitting J between S and T_0. The (0, 2) triplet (not shown) is split off by the much larger intradot exchange energy $J_{(0,2)} \sim 600$ μeV [20] and is inaccessible. Rapid mixing due to hyperfine interaction occurs between states whose energies differ by less than $E_{\rm nuc}$. This occurs at large negative ϵ [lower left of Fig. 1(b)], where S and T_0 mix, and at $J(\epsilon) = E_Z$ [black dot in Fig. 1(b)], where S and T_+ mix.

A cycle of gate configurations is used to prepare and measure two-electron spin states [9], as illustrated in Fig. 1(b). A 200 ns preparation step (denoted P in Fig. 1) configures the dot in (0, 2) at a position where the series $(0, 2)T \rightarrow (0, 1) \rightarrow (0, 2)S$ is energetically allowed and occurs rapidly, giving efficient initialization to a singlet. The gates then shift (waiting 200 ns at P' to reduce pulse overshoot) to a separation point (S) in (1, 1) for a time τ_S during which singlet-triplet evolution occurs. Finally, the gates are set to the measurement point (M) for $\tau_M = 5$ μs, for spin-to-charge conversion. Inside the pulse triangle marked in Fig. 1(c), the triplet states will remain in (1, 1) over the measurement time τ_M [8,21]. Since ~90% of the pulse cycle is spent at M, the relatively slow measurement of the sensor g_s gives a time-averaged charge configuration at the M point. This signal is calibrated to give a singlet state probability $P_S(\tau_S)$ by comparing values within the pulse triangle with values within (1, 1) (which defines $P_S = 0$) and within (0, 2) outside the pulse triangle (which defines $P_S = 1$).

We first measure $J(\epsilon)$, $E_{\rm nuc}$, and V at two values of t_c, allowing the saturation probability $P_S(\infty)$ to be measured as a function of J. This saturation probability is found to depend on the ratio $E_{\rm nuc}/J$ approximately as predicted by theory [16]. We then measure the time evolution $P_S(\tau_S)$, which shows damped oscillations, also in reasonable agreement with theory [16]. $J(\epsilon)$ is measured using the Rabi (or Larmor) sequence described in Ref. [9], in which an adiabatic (compared with $E_{\rm nuc}$) ramp over 1 μs to (1, 1) is used to prepare and measure the electron spin state in the $\{|\uparrow\downarrow\rangle, |\downarrow\uparrow\rangle\}$ basis. An exchange pulse produces coherent rotations with a period t_R [shown in Fig. 2(a)] from which we deduce the exchange coupling $J(\epsilon) = h/t_R$ [22]. Values of $J(\epsilon)$ for small and large t_c are shown in Fig. 2(b), along with a fit to an empirical power-law form $J \propto \epsilon^{-\alpha}$, giving $\alpha \sim 1.4$ [23]. In Fig. 2(c), these values of $J(\epsilon)$ are compared with the results of an alternative method in which rapid dephasing at the S-T_+ degeneracy produces a dip in P_S when the value of ϵ at the S point satisfies $J(\epsilon) = E_Z$. $J(\epsilon)$ can then be measured from a knowledge of the field, using $E_Z = g\mu_B B$, where μ_B is the Bohr magneton, and taking the value $g = -0.44$, measured (using an in-plane field) in a different quantum dot device

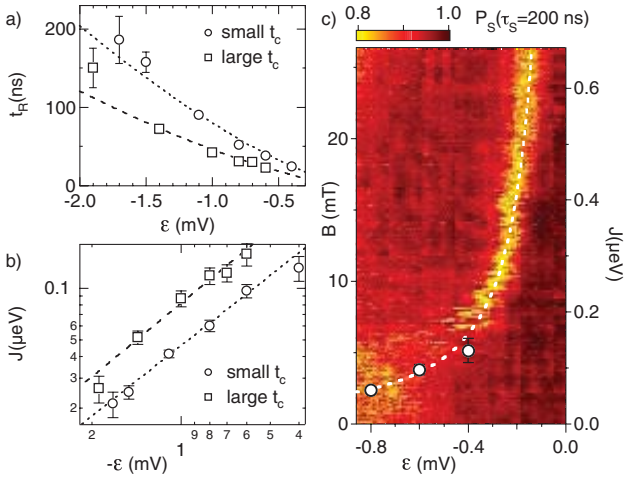

FIG. 2 (color). (a) Period t_R of first Rabi oscillation versus exchange point detuning for small and large tunnel coupling. (b) Exchange energy as a function of detuning, deduced from the data in (a), together with empirical power-law fits $J \propto |\epsilon|^{-1.4\pm0.1}$. t_R corresponding to the fits is shown as curves in (a). (c) Color scale plot of P_S as a function of S-point detuning and magnetic field B obtained using the pulse sequence in Fig. 1(b). The bright band indicates rapid decoherence where $J = g\mu_B B$. The white points and the dashed line are the same data and fits plotted in (b).

made from the same wafer [24]. $J(\epsilon)$ measured by this technique is in qualitative agreement with the power law derived from Fig. 2(b); discrepancies may be due to an anisotropic g-factor or nuclear polarization effects, or may indicate a dependence of $J(\epsilon)$ on field. Since the first method more closely matches the conditions under which data in the rest of this Letter was taken and is more precise in the range of J of interest, we henceforth take $J(\epsilon)$ from Fig. 2(b).

Parameters E_{nuc} and V are extracted from $P_S(\tau_S)$ measured for the S point at large negative ϵ, where $J \ll E_{\mathrm{nuc}}$. In this regime the initial singlet evolves into an equal mixture of singlet and triplet with characteristic time h/E_{nuc}. $P_S(\tau_S)$ for small and large t_c (shown in the insets of Fig. 3) are fit to the form for $P_S^0(\tau_S)$ given in [16], with fit parameters $E_{\mathrm{nuc}} = 45 \pm 3$ neV (47 ± 4 neV), corresponding to hyperfine fields of $\sim$1.8 mT, and $V = 0.53 \pm 0.06$ (0.46 ± 0.06) for small (large) t_c [25]. The fit function $P_S^0(\tau_S)$ depends on J at this detuning, which is too small to measure directly. Instead, $J(\epsilon)$ is extrapolated using the power law from Fig. 2(b); however, the fit parameters are essentially independent of details of the extrapolation, and, for example, are within the error bars for the extrapolation $J \propto |\epsilon|^{-1}$ as well as $J = 0$.

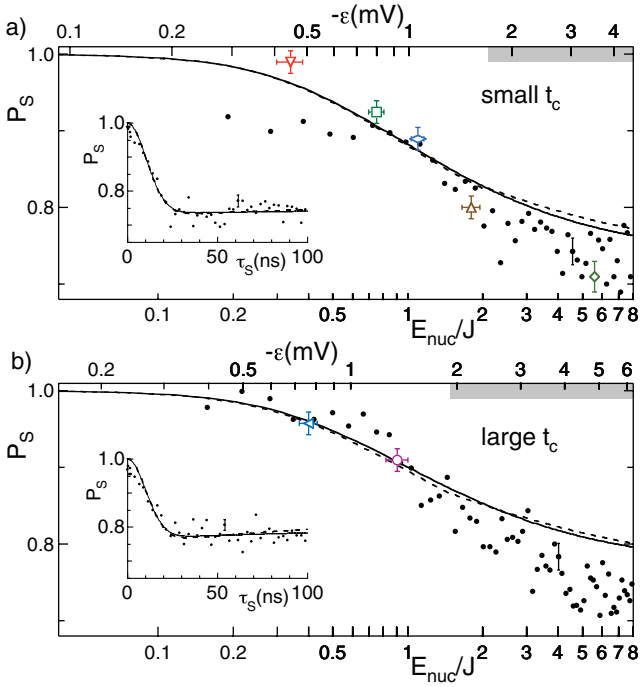

FIG. 3 (color). (a) Inset: $P_S(\tau_S)$ for small t_c and $\epsilon = -5.5$ mV, with fit (see text) giving $E_{\mathrm{nuc}} = 45 \pm 3$ neV and $V = 0.53 \pm 0.06$. Main panel: Measured $P_S(\tau_S = 400\ \mathrm{ns})$ (points) plotted against E_{nuc}/J. Open symbols correspond to P_S in the traces of Fig. 4(a) at the largest τ_S measured for each ϵ. Curve shows theoretical dependence (from [16]) of $P_S(\tau_S \to \infty)$ on E_{nuc}/J, taking into account the measurement fidelity deduced from the inset. The gray bar along the top axis indicates the region where $J(\epsilon)$ is extrapolated (see text). Dashed lines indicate the theoretical predictions (plotted as functions of ϵ) if an alternative extrapolation $J \propto |\epsilon|^{-1}$ is chosen in this region. (b) Large t_c data. The fit to the inset gives $E_{\mathrm{nuc}} = 47 \pm 4$ neV and $V = 0.46 \pm 0.06$, from which the theoretical saturation P_S (curve in main panel) is calculated. Open symbols correspond to the large-τ_S values in Fig. 4(b). Error bars on the solid symbols show the uncertainty in P_S arising from charge noise in the sensing point contact.

$P_S^0(\tau_S)$ is expected to show a range of interesting behavior depending on the relative magnitudes of J and E_{nuc} [16]: In the limit $J = 0$, $P_S^0(\tau_S \to \infty)$ rapidly saturates to $1/2$. As J is increased, hyperfine dephasing becomes less effective, with $P_S^0(\infty)$ saturating at progressively higher values, approaching unity when $J \gg E_{\mathrm{nuc}}$, and following a universal function of E_{nuc}/J. As a function of τ_S, $P_S^0(\tau_S)$ is predicted to undergo damped oscillations, which when plotted versus $\tau_S J$ follow another universal function of E_{nuc}/J and exhibit a universal phase shift of $3\pi/4$ at large $\tau_S J$.

Knowing $J(\epsilon)$ and E_{nuc} allows the long-time ($\tau_S \gg h/J$) saturation of the measured P_S to be compared with theory [16]. We set $\tau_S = 400$ ns and sweep the position of the S point. For small and large t_c, $P_S(400\ \mathrm{ns})$ is plotted in Fig. 3 as a function of E_{nuc}/J, where E_{nuc} is obtained from the fits described above and $J(\epsilon)$ are taken from Fig. 2. At the most negative detunings (in the regions marked by gray bars in Fig. 3) J is too small to be measured by either Rabi period or S-T_+ degeneracy methods; instead, $J(\epsilon)$ is found by extrapolating the power-law fits. As above, agreement with theory (discussed below) is insensitive to the details of the extrapolation, as shown by the dashed lines in Fig. 2.

The long-τ_S P_S data shown in Fig. 3 agree fairly well with the saturation values predicted from [16], taking into account the visibility (assumed independent of ϵ) obtained from the insets. In particular, P_S has the same dependence on E_{nuc}/J at both values of t_c measured, even though the function $J(\epsilon)$ depends on t_c. P_S is up to $\sim$0.06 smaller than predicted at the largest detunings; both cotunneling and nuclear decorrelation over the duration of the separation pulse tend to equalize singlet and triplet occupations, although it is unclear whether they are the cause of this effect.

We next investigate the time dependence of $P_S(\tau_S)$ at finite J. For five (two) S-point detunings at small (large) t_c, $P_S(\tau_S)$ was measured out to $\tau_S J/\hbar \approx 15$. The results are shown in Fig. 4, together with the predicted time evolution from [16] with values for V and E_{nuc} taken from fits shown in the insets of Fig. 3. Because P_S remains close to unity, these data are particularly sensitive to calibration imperfections caused by quantum point contact nonlinearities and noise in the calibration data, whose effect to lowest order is to shift the data vertically. Traces in Fig. 4 are therefore shifted vertically to satisfy the constraint $P_S(\tau_S = 0) = 1$. In no case was this greater than ± 0.05. Here and in Fig. 3, the error bars reflect uncertainty in P_S from charge noise in the sensing point contact; additional scatter in the data may be due to long nuclear correlation times [9,13].

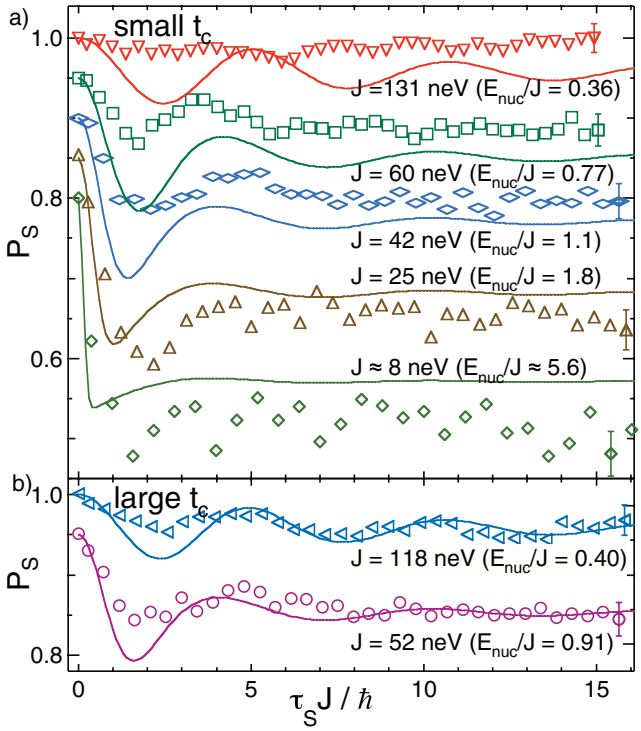

FIG. 4 (color). (a) Symbols: Experimental $P_S(\tau_S)$ at small t_c for various J, plotted as a function of $\tau_S J/\hbar$. Curves: Predictions from [16] using $E_{\rm nuc}$ and V fit from Fig. 3(a). Adjacent traces after the first are offset by 0.05 for clarity. (b) Corresponding data and theory for large t_c. Lower trace is offset by 0.05 for clarity. Error bars reflect the contribution of sensor charge noise.

Damped oscillations are observed as predicted in [16]; however, even after taking into account the empirical visibility factor, the amplitude of the oscillations is less than expected. This is likely due to the finite rise time of the separation pulse and to switching noise, which make each trace effectively an average over a range of J values. Where the amplitude is large enough for the period and phase of the oscillations to be made out, these approximately match the predictions of [16], although with two significant departures: The topmost trace, with smallest $E_{\rm nuc}/J$, does not show clear oscillations, and the expected shift of the first minimum to smaller $\tau_s J$ at intermediate J is not observed. We do not understand the origin of these effects. The amplitude of the oscillations falls off too rapidly for the expected $3\pi/4$ phase shift at large $\tau_S J$ to be visible. Similar oscillations of P_S are predicted close to the S-T_+ degeneracy with a characteristic frequency $\sim\Delta = J - E_Z$. We have searched for these oscillations but do not observe them. We believe the reason for this is that Δ varies much more rapidly with ϵ in this region than J does at the S-T_0 near degeneracy; the oscillations are therefore washed out by switching noise and pulse overshoot.

In summary, after including the measured readout efficiency, we find that the singlet correlator shows damped oscillations as a function of time and saturates at a value that depends only on $E_{\rm nuc}/J$. Both these features are qualitatively as expected from theory [16]; some of the departures from expected behavior may be qualitatively accounted for by cotunneling and nuclear decorrelation (which tend to equalize singlet and triplet probabilities at long times) and charge noise (which tends to smear out the oscillations seen in Fig. 4.)

We acknowledge useful discussions with W. Coish, H. A. Engel, D. Loss, M. Lukin, and J. M. Taylor. This work was supported by DARPA-QuIST and the ARO/ARDA/DTO STIC program.

[1] D. Loss and D. P. DiVincenzo, Phys. Rev. A **57**, 120 (1998).
[2] J. M. Taylor *et al.*, Nature Phys. **1**, 177 (2005).
[3] T. Fujisawa *et al.*, Nature (London) **419**, 278 (2002).
[4] J. M. Elzerman *et al.*, Nature (London) **430**, 431 (2004).
[5] A. S. Bracker *et al.*, Phys. Rev. Lett. **94**, 047402 (2005).
[6] P.-F. Braun *et al.*, Phys. Rev. Lett. **94**, 116601 (2005).
[7] R. Hanson *et al.*, Phys. Rev. Lett. **94**, 196802 (2005).
[8] A. C. Johnson *et al.*, Nature (London) **435**, 925 (2005).
[9] J. R. Petta *et al.*, Science **309**, 2180 (2005).
[10] S. I. Erlingsson, Y. V. Nazarov, and V. I. Fal'ko, Phys. Rev. B **64**, 195306 (2001); I. A. Merkulov, A. L. Efros, and M. Rosen, Phys. Rev. B **65**, 205309 (2002); A. V. Khaetskii, D. Loss, and L. Glazman, Phys. Rev. Lett. **88**, 186802 (2002).
[11] J. Levy, Phys. Rev. Lett. **89**, 147902 (2002).
[12] K. Ono and S. Tarucha, Phys. Rev. Lett. **92**, 256803 (2004).
[13] F. H. L. Koppens *et al.*, Science **309**, 1346 (2005).
[14] J. Nicholas Turro, Proc. Natl. Acad. Sci. U.S.A. **80**, 609 (1983); A. L. Buchachenko, J. Phys. Chem. A **105**, 9995 (2001).
[15] H. Staerk *et al.*, Chem. Phys. Lett. **118**, 19 (1985); V. F. Tarasov *et al.*, J. Am. Chem. Soc. **114**, 9517 (1992).
[16] W. A. Coish and D. Loss, Phys. Rev. B **72**, 125337 (2005).
[17] M. Field *et al.*, Phys. Rev. Lett. **70**, 1311 (1993).
[18] J. M. Elzerman *et al.*, Phys. Rev. B **67**, 161308 (2003).
[19] L. DiCarlo *et al.*, Phys. Rev. Lett. **92**, 226801 (2004).
[20] A. C. Johnson *et al.*, Phys. Rev. B **72**, 165308 (2005).
[21] J. R. Petta *et al.*, Phys. Rev. B **72**, 161301(R) (2005).
[22] When $J \lesssim E_{\rm nuc}$, J must be corrected downwards slightly because precession in the nuclear field enhances the average Rabi frequency. The correction to J never exceeds 13%.
[23] A simple level anticrossing with t_c and ϵ independent would give $J \propto \epsilon^{-1}$. The discrepancy may be due to a detuning-dependent t_c.
[24] D. M. Zumbühl *et al.*, Phys. Rev. Lett. **93**, 256801 (2004).
[25] The dependence of V on t_c is not understood. The effect of alternative visibility parameters on the predictions of Figs. 3 and 4 is simply to scale them towards or away from $P_S = 1$.